Editors' Suggestion

Geometrical frustration and piezoelectric response in oxide ferroics

Valeri Petkov,[1] Jong-Woo Kim,[2] Sarvjit Shastri,[2] Shashaank Gupta,[3] and Shashank Priya[4]

[1]*Department of Physics and Science of Advanced Materials Program, Central Michigan University, Mt. Pleasant, Michigan 48859, USA*

[2]*X-ray Science Division, Advanced Photon Source, Argonne National Laboratory, Argonne, Illinois 60439, USA*

[3]*Virginia Tech India Center for Advanced Research and Education, Chennai, Tamil Nadu 600095, India*

[4]*Department of Materials Science and Engineering, Penn State, University Park, Pennsylvania 16802, USA*

(Received 24 September 2019; published 13 January 2020)

Materials with increased functionality are often based on crystalline structures with significant local disorder. Typical examples are ferroic oxides exhibiting large spontaneous polarization that can be rotated by an applied electric field, finding use in many important applications. Despite years of investigation, the exact structural origin of the increased piezoelectric response of oxide ferroics is still unclear. Frequently evoked models attribute it to emerging polar nanoregions inside a nonpolar matrix, the existence of a morphotropic boundary separating polar phases with different crystallographic symmetry, low-symmetry bridging phases facilitating polarization rotation, and displacive and order-disorder structural phase transitions. Here we use both conventional and resonant high-energy x-ray diffraction coupled to atomic pair distribution function analysis and three-dimensional computer simulations to examine the relationship between the local structure and piezoelectric properties of exemplary sodium-potassium niobate ferroics. We show that their increased piezoelectric response is primarily due to a geometrical frustration in the underlying perovskite lattice induced by local fluctuations in the tilt pattern of the constituent niobium-oxygen octahedra, and not to a crystal-crystal phase transition or distinct nanodomains. The fluctuations peak when the sodium to potassium ratio approaches 1, leading to a softening of the perovskite lattice and easing of polarization rotation under an electric field. Based on the experimental data and model calculations involving Goldschmidt's tolerance factor for the stability of perovskites, we also show that the fluctuations are driven by the mismatch between the radii of sodium and potassium atoms, and the increased piezoelectric response of sodium-potassium niobates indeed scales with the variance in the distribution of these radii about the average value. Thus, we settle important aspects of the debate over the structure-piezoelectric property relationship for oxide ferroics, thereby providing a different perspective on the ongoing effort to improve their useful properties.

DOI: 10.1103/PhysRevMaterials.4.014405

I. INTRODUCTION

Sodium-potassium niobates, $Na_{1-x}K_xNbO_3$ (KNNs), are a viable alternative to Pb-containing ferroelectric oxides that dominate the actuator and high-power transducer applications [1–3]. The parent compounds of KNNs exhibit a perovskite-type structure, rich polymorphisms, and distinct ferroelectric properties. In particular, $KNbO_3$ is rhombohedral (**R**; *S.G. R3m*) at low temperatures (< -10 °C), it is orthorhombic (**O**; *S.G. Amm2*) at room temperature, it adopts a tetragonal structure (**T**; *S.G. P4mm*) at elevated temperature (200–400 °C), and it becomes cubic (**C**; *S.G. Pm-3m*) when the temperature is increased further (> 400 °C) [4–6]. Two competing models for the nature of the phase transitions in $KNbO_3$ have been put forward. One of the models assumes that the **C** → **T**, **T** → **O**, and **O** → **R** transitions are accompanied by displacement of Nb atoms along a fourfold, twofold, and threefold symmetry axis of the aristotype cubic lattice, respectively. The displacement, also known as Nb off-centering, renders **T**, **O**, and **R** polymorphs ferroelectric. On the other hand, the order-disorder model of the transitions assumes that Nb-O octahedra in $KNbO_3$ are those observed in the **R** polymorph, and hence only in that polymorph are the octahedra equivalent at any instant. In the higher-temperature polymorphs, they are equivalent on average, while at any instant the direction of Nb off-centering in different octahedra is different. Recent studies have shown that in $KNbO_3$, both scenarios are likely to occur, and a crossover from mostly displacive to order-disorder structural transitions takes place with increasing temperature [4–7]. The atomic structure of $NaNbO_3$ is even more complex. It has been reported to have at least seven polymorphs, and, furthermore, the structure of some of them is still under debate. The technologically important room-temperature polymorph of $NaNbO_3$ is considered to be orthorhombic (*S.G. Pbcm*) and antiferroelectric [8]. However, studies have also argued that the polymorph has a lower crystallographic symmetry (e.g., monoclinic *S.G. Pm*) or even that it is a mixture of two orthorhombic phases (centrosymmetric *S.G. Pbcm* and noncentrosymmetric *S.G.* $P2_1ma$) [9,10]. The complexity of the structure of $NaNbO_3$ arises from tilting of Nb-O octahedra induced by the relatively small size of Na atoms (ionic Na^+ radius 1.39 Å) positioned in the 12-fold-coordinated cavities between the octahedra [11,12]. The larger K cations (ionic K^+ radius 1.64 Å) fit the cavities well, and tilts are not observed with $KNbO_3$. Octahedral tilts in perovskites may also be associated with the so-called Goldschmidt's tolerance factor, t, used to evaluate their geometrical stability and distortion at atomic level [13,14]. As numerous studies have shown, tilts

may appear when t is below 1, and they are not observed for $t \geqslant 1$ [14]. For reference, values of t for $NaNbO_3$ and $KNbO_3$ are 0.96 and 1.06, respectively. Due to their common perovskite-type structure and specific tolerance factors, the parent compounds of $Na_{1-x}K_xNbO_3$ ferroics form stable solid solutions exhibiting excellent piezoelectric properties in the vicinity of $x = 0.5$ [4–8]. It is often considered that the phase diagram of KNNs is dominated by K, and hence at room temperature, the structure of KNNs would possess the crystallographic symmetry of the **O** polymorph of $KNbO_3$ (*S.G. Amm2*). However, powder x-ray diffraction (XRD) experiments have clearly shown that octahedral tilts exist for all solid solutions in the Na-rich side of the KNN phase diagram. Furthermore, the experiments have indicated that the atomic structure of KNNs may also be described as monoclinic (*S.G. Pm)* [15,16]. The apparent structural complexity of KNNs has made it difficult to understand the increase in their piezoelectric response in comparison to the parent compounds [3–5]. Here we obtain the missing knowledge by performing advanced x-ray scattering experiments and three-dimensional (3D) structure modeling. Our findings provide a coherent picture of the piezoelectric properties of KNNs that is likely to be relevant to many complex ferroelectric oxides of the perovskite family.

II. HIGH-ENERGY X-RAY DIFFRACTION AND 3D STRUCTURE MODELING

To examine the atomic structure of KNN in detail, a series of KNN single crystals with the chemical formula $Na_{1-x}K_xNbO_3$ ($x = 0$, 0.16, 0.42, 0.52, 0.53, 0.82, and 1) were grown by the flux method [17]. Details are given as Supplemental Material [18]. The crystals were grinded into fine powders and subjected to high-energy x-ray diffraction (XRD) experiments coupled to atomic pair distribution function (PDF) analysis. The experiments were optimized to achieve high resolution in both reciprocal and real space (see Figs. S1, S2, and S3 and related text in the Supplemental Material [18]). The technique has proven useful in structure studies of crystalline materials with local structural disorder [19,20]. Experimental details are given in the Supplemental Material [18]. Rietveld analysis of the synchrotron XRD patterns (see Fig. S1 in the Supplemental Material [18]) showed that the atomic arrangement in KNNs may be well described in terms of an orthorhombic structure model (*Space Group* (*S.G.*) *Amm2*). However, except for the parent compounds, Rietveld fits of good quality were also obtained using a monoclinic structure model (*S.G. Pm*). The ambiguous outcome of Rietveld analysis can be attributed to the limited ability of sharp Bragg peak-based crystallography to clearly reveal local structural disorder. High-resolution atomic PDFs derived from the patterns are shown in Fig. 1. In line with the results of Rietveld analysis, crystal structure constrained fits to the PDFs indicate that KNNs exhibit a perovskite-type structure with an average orthorhombic symmetry (see Fig. S4 in the Supplemental Material [18]). Inspection of the PDFs in Figs. 1(a) and 1(b) provides more structural details. In particular, it reveals that Nb-O octahedra forming the perovskite lattice of KNNs are organized in approximately 2-nm-sized configurations that evolve subtly with the Na-to-K ratio. On the other hand, features characteristic of the average crystal structure of KNNs, which dominate the PDF signal above 2 nm, evolve markedly with that ratio. The observation indicates significant divergence of the local structure of KNNs from the average crystal structure. In this respect, the experimental PDFs for KNNs resemble very much those for $Ga_{1-x}In_xAs$ solid solutions, where the local and average crystal structure also diverge [21]. The difference is that the building units of $Ga_{1-x}In_xAs$ solid solutions are alternating Ga-As and In-As atomic pairs forming a continuous diamond-type lattice, whereas those of $Na_{1-x}K_xNbO_3$ solid solutions are Nb-O octahedra forming a continuous perovskite-type lattice whose cavities are occupied by either Na or K atoms. Furthermore, data in Fig. 1(c) show that the closer the Na-to-K ratio is to 1, the shorter is the coherence length of the underlying perovskite-type lattice.

The presence of distinct local and average structure makes the description of the structure-property relationship for KNNs in terms of a single crystallographic cell less detailed. Therefore, we explored large-size models refined against both XRD patterns and atomic PDFs. The approach has already proven very useful in structure studies of complex systems [22–24]. Atomic PDFs for a multicomponent material, however, show all distinct correlations between the constituent atoms. In the case of KNNs, those are alkali-metal–alkali-metal, alkali-metal–Nb, Nb-Nb, Nb-O, and O-O atomic correlations. The correlations appear as PDF peaks that often overlap, rendering the interpretation of the experimental data difficult (see Fig. S5 in the Supplemental Material [18]). As numerous studies have shown, a major factor contributing to the spontaneous polarization of KNNs is the Nb off-centering [3–5]. Therefore, to obtain diffraction data with increased sensitivity to atomic pair correlations involving Nb, we conducted resonant high-energy XRD experiments at the K edge of Nb. The technique involves collecting data sets using x rays with energy close to and a few hundred eV below the K edge of Nb and taking the difference between the respective sets (see Fig. S6 in the Supplemental Material [18]). The Fourier transform of the difference, the so-called Nb-differential atomic PDF, reveals only Nb–alkali-metal, Nb-Nb, and Nb-O atomic correlations in KNNs, i.e., the number of distinct peaks contributing to its profile is reduced considerably in comparison to the respective total PDF (see Fig. S7 in the Supplemental Material [18]). An added advantage is that the contribution of Nb-Nb and Nb-O correlations to Nb-differential PDFs is ~50% and 30%, respectively, i.e., very significant. This is important because, as discussed below, knowledge of bond distances and angles involving Nb and oxygen atoms allows us to determine the evolution of the local structure of KNNs with their composition in fine detail. For reference, the contribution of Nb-Nb correlations to total PDFs for KNNs is ~ 30% only. In this respect, differential atomic PDFs appear similar to results of extended x-ray absorption fine-structure (EXAFS) experiments. Unlike EXAFS, which yields atomic ordering information out to 5–6 Å, differential PDFs show atomic correlations up to the longest interatomic distances to which they extend [25,26]. This facilitates exploring atomic-pair correlations of interest well-beyond the first atomic coordination sphere. More details about the resonant high-energy XRD experiments and derivation of differential atomic PDFs are given in the Supplemental Material [18].

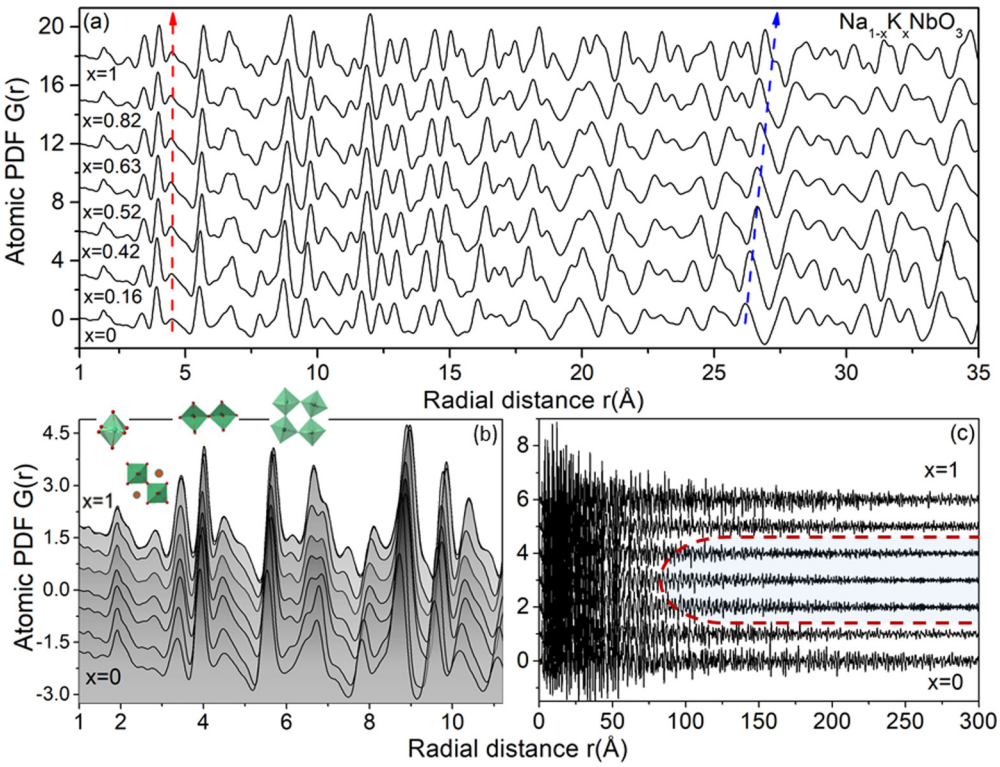

FIG. 1. (a) Experimental total atomic PDFs for $Na_{1-x}K_xNbO_3$ ferroics ($x = 0$, 0.16, 0.42, 0.52, 0.63, 0.82, and 1). Arrows emphasize the subtle (red arrow) and marked (blue arrow) evolution of the local and average structure of KNNs with their compositions. (b) Low-r region of the PDFs indicating the presence of fairly rigid Nb-O_6 octahedra (PDF peak at about 1.9 Å marked with a single octahedron), increasing positional order of alkali-metal atoms with K percentage (emerging PDF peak at about 2.8 Å marked with two octahedra and nearby alkali-metal atoms), hardly changing distances between Nb atoms centering adjacent octahedra (PDF peak at about 4 Å marked with corner sharing octahedra) and subtle evolution of the next-nearest-neighbor atomic correlations including octahedral tilts (PDF peak at about 6.9 Å marked with four tilted octahedra). (c) Higher-r region of the PDFs indicating the limited range of structural coherence in KNNs in comparison to the parent compounds (see the accelerated decay of the respective PDFs with interatomic distances outlined with a red broken line).

Three-dimensional (3D) structure models for the studied KNNs were constructed and tested against the respective XRD patterns, total and Nb-differential PDFs. The models comprised about 120 000 atom configurations with a cubelike shape and edge with a length of about 10 nm. This is also important because KNNs in which the Na-to-K ratio approaches 1 are seen to exhibit not only different local and average atomic structure but also a limited degree of structural coherence [∼8 nm; see Fig. 1(c)]. The size of the models allows us to explore and relate these striking structural characteristics of KNNs to their piezoelectric properties. Models with the structure of the **C, T, O,** and **R** polymorphs of $KNbO_3$ and the room-temperature polymorph of $NaNbO_3$ (*S.G. Pbcm*) were tested. Models with an average monoclinic symmetry (*S.G. Pm*) were also tested. The models with an average **O**-type structure appeared suitable for $Na_{1-x}K_xNbO_3$ with $x = 0.42$, 0.53, 0.82, and 1. The monoclinic type models appeared suitable for $Na_{1-x}K_xNbO_3$ with $x = 0.16$ and 0.42. As may be expected, a model based on the room-temperature polymorph of $NaNbO_3$ appeared suitable for $Na_{1-x}K_xNbO_3$ with $x = 0$, although to a lesser extent the model also appeared suitable for $Na_{0.84}K_{0.16}NbO_3$. The models that emerged from the tests as most plausible were refined to the maximum possible extent using a combination of Rietveld and reverse Monte Carlo computational techniques. More details of the 3D structure modeling are given in the Supplemental Material [18]. Fragments of the most successful structure models for KNNs are shown in Fig. 2. Total and Nb-differential PDFs computed from the models are compared with the experimental data in Figs. 3 and 4, respectively.

III. ANALYSIS OF THE 3D STRUCTURE MODELS

In analyzing a series of large-size atomistic models for a composition dependence of structural features, sensible reference points are needed. As such, we used the room-temperature **O** polymorphs of the parent compounds of KNNs, i.e., the **O** polymorph of $NaNbO_3$ (*S.G. Pbcm*) and $KNbO_3$ (*S.G. Amm2*). Indeed, their structure appeared as the most successful approximation to the experimental diffraction data for $Na_{1-x}K_xNbO_3$ with $x = 0$ and 1, respectively. Fragments of the ideal structures of the polymorphs, revealing well their local characteristics, are shown in Figs. 5 and 6. In the **O**-polymorph of $KNbO_3$, Nb-O octahedra are not tilted with respect to each other, and K atoms experience a unique 12-fold oxygen coordination, resulting in identical K-O bonding distances. Furthermore, Nb atoms are displaced toward the midpoint of a basal

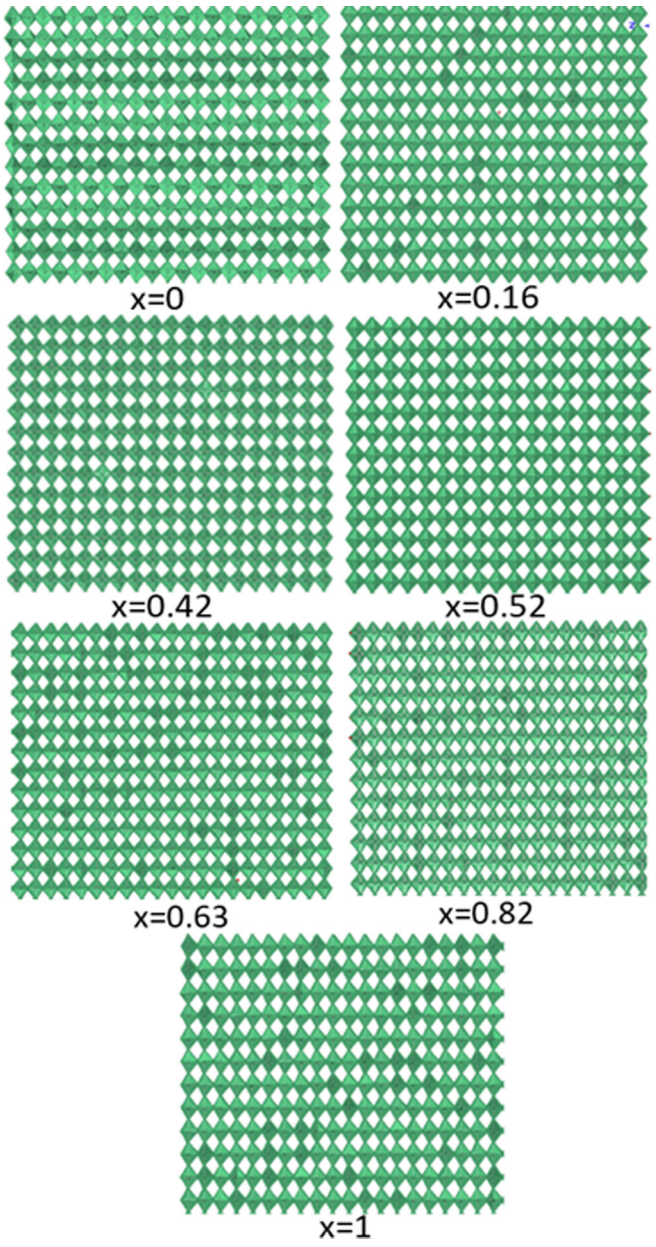

FIG. 2. Fragments from the refined 3D models for $Na_{1-x}K_xNbO_3$ ferroics ($x = 0$, 0.16, 0.42, 0.52, 0.63, 0.82, and 1) emphasizing the corner connectivity of the constituent Nb-O octahedra (green) as assembled in a continuous perovskite-type lattice. The models differ in fine details discussed in Figs. 4–6.

edge of the octahedra, which is the direction of spontaneous polarization. Hence, there are two long (∼2.22 Å) and two short (∼1.89 Å) Nb basal oxygen (O_{bas}) bonds, while bonds between Nb and apical oxygens (O_{ap}) are approximately 2.02 Å long. The Nb-O_{bas}-Nb and Nb-O_{ap}-Nb bond angles are approximately 173° and 167°, respectively. The small deviation from 180° is due to the significant Nb off-centering. In the **O** polymorph of $NaNbO_3$, Nb-O octahedra are tilted appreciably with respect to each other, and Na atoms experience two types of oxygen coordination, resulting in a broad distribution of Na-O bonding distances. Furthermore, contrary to the case of $KNbO_3$, the basal planes of nearby octahedra in $NaNbO_3$ are not coplanar, rendering the distribution of O-Nb-O bond angles rather broad. In particular, Nb-O_{bas}-Nb bond angles range from approximately 155° to 167° and Nb-O_{ap}-Nb angles deviate from 180° considerably, ranging from 146° to 161°. This observation is not a surprise because, in general, when the *A*-site cation in ABO_3 perovskites, i.e., Na, is relatively small, tilts would appear as the lowest energy distortion mode to satisfy its coordination preference and relieve the associated "positive chemical pressure" on the perovskite network. At the same time, the coordination sphere of the *B*-site cation, i.e., Nb-O octahedra, would remain largely undisturbed, and only the usually soft *B*-O-*B* angles, i.e., O-Nb-O angles, over the coupling of the oxygen octahedra would bend [11,12]. Here, on average, the off-centering of Nb atoms is asymmetric with respect to O_{bas}, leading to four Nb-O_{bas} distances ranging from 1.86 to 2.11 Å. However, bonds between Nb and O_{ap} are of a nearly equal length (∼1.98 Å). Thus, Nb off-centering in $NaNbO_3$ appears intermediate between the one-corner (⟨001⟩ direction) and two-corner (⟨011⟩ direction) Nb off-centering in the **T** and **O** polymorphs of $KNbO_3$, respectively. The specific octahedral tilt pattern and Nb off-centering in $NaNbO_3$ render it antiferroelectric merely because polar displacements in successful pairs of octahedral layers appear out-of-phase [3,8].

Studies have shown that a moderate doping of $NaNbO_3$ with K expands the cavities of the perovskite lattice and reverses the tilts of Nb-O octahedra. This changes the sense of Nb off-centering, rendering it closer to that in the **O** polymorph of $KNbO_3$. As a result, KNNs in the Na-rich size of the phase diagram exhibit diminishing octahedral tilts with K percentage and behave as ferroelectrics [4,15,16]. Notably, the type of Nb off-centering in KNNs does not seem to influence significantly the overall shape of Nb-O octahedra. In particular, both the Nb-O_{ap} bonds and the average Nb-O bond distance ($\{4 * \text{Nb-O}_{bas} + 2 * \text{Nb-O}_{ap}\}/6$) in $KNbO_3$ and $NaNbO_3$ appear rather similar. Furthermore, bond angles involving oxygens occupying the corners of Nb-O polyhera, i.e., O_{ap}-O_{bas}-O_{ap} and O_{bas}-O_{bas}-O_{bas} angles, are close to 90°. Evidently, Nb-O octahedra in KNNs are fairly rigid, hence changes in their tilts with K percentage cause nearby Na atoms to reposition so as to avoid the formation of unacceptably short Na-O distances. The effect of reorientation of Nb-O octahedra and repositioning of Na atoms in KNNs with $x \sim 0.5$ on their piezoelectric properties has been discussed in Ref. [27]. Altogether, Nb and oxygen involving bonding distances and angles in the parent compounds appear as appropriate reference points for evaluating the evolution of the octahedral tilt pattern and related Nb off-centering in KNNs with their composition.

Distribution of Nb-O_{bas} and Nb-O_{ap} bonding distances in KNNs as a function of their composition, as extracted from the respective 3D models, is shown in Fig. 7. As can be seen in the figure, Nb-O_{bas} distances in $NaNbO_3$ show a broad distribution due to the asymmetric displacement Nb atoms with respect to the basal oxygens. The distribution becomes less irregular with K percentage and splits into two well-defined peaks characteristic of the Nb off-centering in the **O** polymorph of $KNbO_3$. Angles along the diagonal of the basal plane of Nb-O octahedra (O_{bas}-Nb-O_{bas}) also evolve toward acquiring their values in $KNbO_3$. At the same time, on

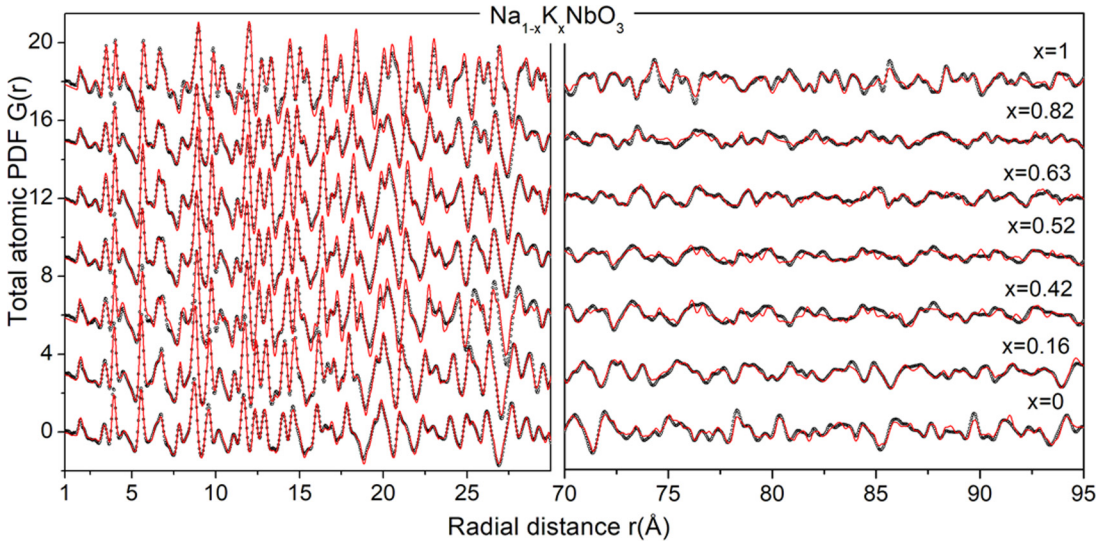

FIG. 3. Experimental (symbols) and RMC fit (red line) total atomic PDFs for $Na_{1-x}K_xNbO_3$ ferroics ($x = 0$, 0.16, 0.42, 0.52, 0.63, 0.82, and 1). The level of agreement between the experimental and computed data is on the order of 15%, i.e., very good [18,19].

average, Nb-O_{ap} distances change little. Evidently, while its average magnitude does not seem to change significantly with K percentage remaining close to 0.2 Å, the direction of Nb off-centering in KNNs, which is indicative of the direction of spontaneous polarization, gradually lines up with that of Nb off-centering in the **O**-polymorph of $KNbO_3$. Concurrently, on average, tilts of Nb-O octahedra diminish, as indicated by the evolution of the average Nb-O_{ap}-Nb and Nb-O_{bas}-Nb bond angles (see Fig. 7, right). However, contrary to the findings of traditional XRD [15,16], atomic PDF analysis indicates that the tilts do not disappear completely when the Na-to-K ratio approaches 1 but merely cease to be correlated over long-range distances. In particular, local configurations of octahedra exhibiting a tilt pattern different from that exhibited by the majority octahedra in the respective KNN model, e.g., a tilt pattern characteristic of $NaNbO_3$ in K-rich models and no tilts in Na-rich models, can be identified clearly in the model perovskite lattices shown in Fig. 8. The configurations are rather fuzzy, i.e., they do not have well-defined boundaries, and, in this sense, they may not be considered as distinct domains. Rather, they may be described as local fluctuations in octahedral tilts, i.e., local structural disorder, which break the average crystallographic symmetry in KNNs and significantly reduce the coherence length of the underling perovskite lattice. Notably, the local structural disorder is seen to peak when the Na-to-K ratio in KNNs approaches 1. The disorder can be revealed by atomic PDF analysis but averages out over long-range distances. Hence, it is difficult to be detected by traditional XRD. A similar scenario has been suggested by Glazer *et al.* when considering the "missing" morphotropic boundary in $Pb(Zr_{1-x}Ti_x)O_3$ ferroics [22,28].

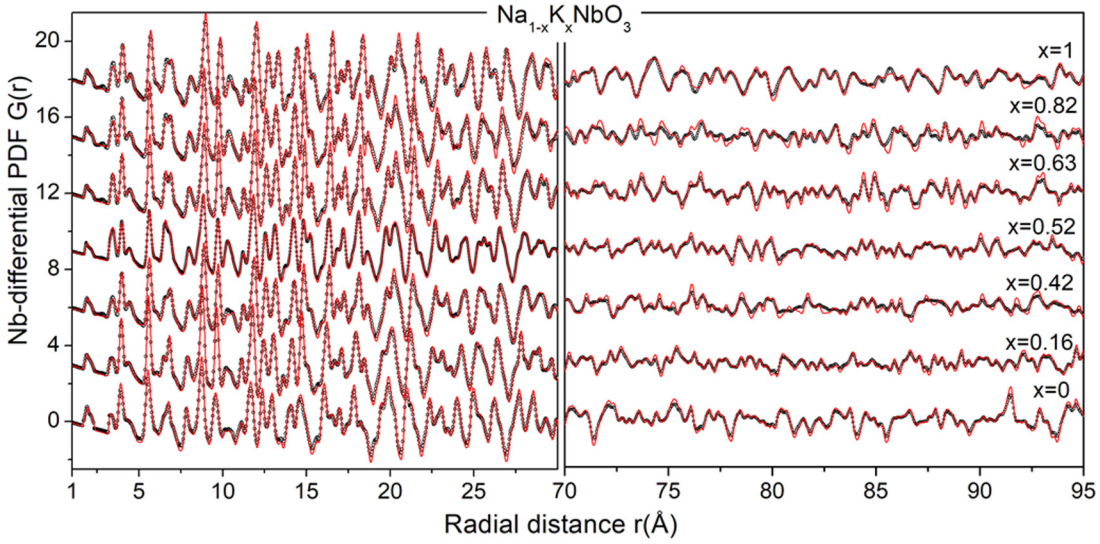

FIG. 4. Experimental (symbols) and RMC fit (red line) Nb-differential PDFs for $Na_{1-x}K_xNbO_3$ ferroics ($x = 0$, 0.16, 0.42, 0.52, 0.63, 0.82, and 1). The level of agreement between the experimental and computed data is on the order of 19%, i.e., very good [19,20].

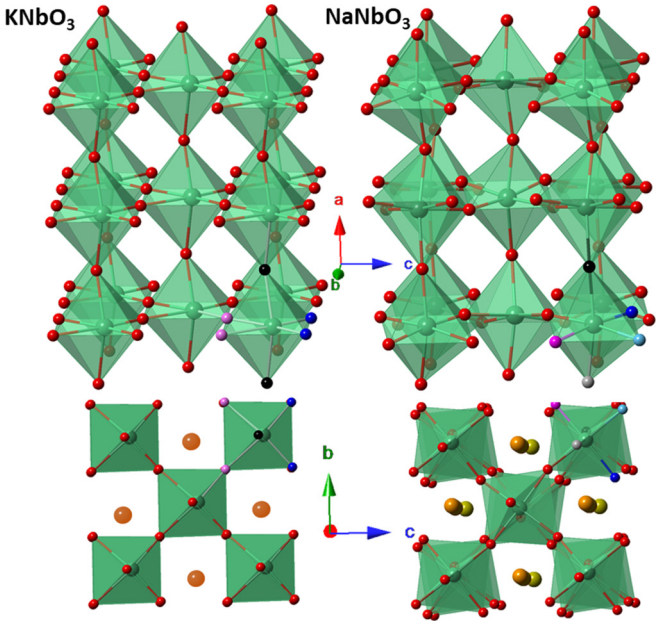

FIG. 5. Atomic structure of the room-temperature polymorphs of $KNbO_3$ (*S.G. Amm2*) and $NaNbO_3$ (*S.G. Pbcm*). For simplicity, both structures are projected on the same *a*, *b*, and *c* axes of an orthorhombic lattice, where the axes are perpendicular to each other and inequivalent in length. Both structures feature a perovskite-type lattice of Nb-O_6 octahedra (green), where K and Na atoms occupy 12-fold-coordinated cavities between the octahedra. Also, in both structures Nb atoms are displaced from the center of Nb-O_6 octahedra. However, contrary to the case of $KNbO_3$, the Nb-O_6 octahedra in $NaNbO_3$ are tilted with respect to each other. Hence, K atoms in $KNbO_3$ occupy one (orange) whereas Na atoms in $NaNbO_3$ occupy two different Wyckoff positions (orange and light green), i.e., they experience two different types of oxygen environment.

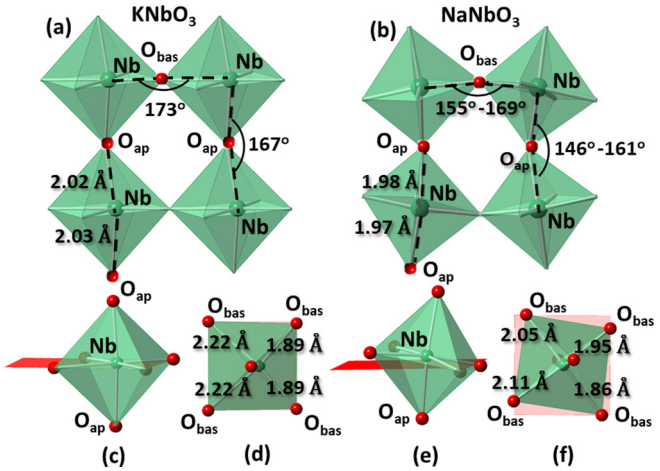

FIG. 6. Fragments from the room-temperature polymorphs of $KNbO_3$ (a) and $NaNbO_3$ (b). Note that the fragments are projected on the same *a*, *b*, and *c* axes of an orthorhombic lattice. Nb-O_6 polyhedra in $KNbO_3$ are not tilted with respect to each other (c). Hence, both Nb-O_{bas}-Nb and Nb-O_{ap}-Nb bond angles are close to 180°. The deviation from 180° is due to the off-centering of Nb atoms. Nb-O_6 octahedra in $NaNbO_3$ are tilted with respect to each other (e). Hence, both Nb-O_{bas}-Nb and Nb-O_{ap}-Nb angles are not only considerably different from 180° but also show a broad distribution. In $KNbO_3$, Nb off-centering is symmetric with respect to the basal oxygens (d) leading to two short (∼1.89 Å) and two long Nb-O_{bas} distances (∼2.22 Å). In $NaNbO_3$, Nb off-centering is asymmetric with respect to the basal oxygens (f) leading to four different Nb-O_{bas} distances, ranging from 1.86 to 2.11 Å. In this respect it appears intermediate between the one-corner ⟨001⟩ Nb off-centering in tetragonal $KNbO_3$ (Nb moves toward O_{ap}) and two-corner ⟨110⟩ Nb off-centering in orthorhombic $KNbO_3$ (Nb moves toward the midpoint of a basal edge of Nb-O_6 octahedra). However, the Nb-O_{ap} bonds and average Nb-O bond distance, Nb-O(average) = $\{4 * (\text{Nb-O}_{bas}) + 2 * (\text{Nb-O}_{ap})\}/6$ in $KNbO_3$ and $NaNbO_3$, are similar. Furthermore, in both materials O_{bas}-O_{bas}-O_{bas} and O_{ap}-O_{bas}-O_{ap} bond angles are close to 90°. Evidently, the shape of Nb-O_6 octahedra in KNNs is not much influenced by the particular off-centering of Nb atoms, i.e., the octahedra are fairly rigid. Red rectangles in (c), (d), (e), and (f) represent the (100) plane of the orthorhombic lattice in the selected setting of lattice vectors ***a***, ***b***, and ***c***. Plots in (d) and (f) represent the base of Nb-O_6 octahedra projected onto the (100) plane.

IV. STRUCTURE-FUNCTION RELATIONSHIP FOR KNN FERROICS

Experimental data for the piezoelectric constant, average unit cell volume, bond angles sensitive to octahedral tilts, related Nb off-centering, and length of structural coherence in KNNs are summarized in Fig. 9 (left) as a function of their composition. All quantities evolve nonlinearly with the Na to K ratio. In particular, the average unit cell volume and piezoelectric constant reach their maximum values and the coherence length reaches its minimum value when that ratio approaches 1. Then, the following picture for the increased piezoelectric response of KNNs emerges. When K replaces Na in the cavities of the perovskite lattice, the lattice would expand because of the larger size of K in comparison to Na atoms. The expansion would take place largely by reducing the tilts of octahedra surrounding a "guest" K atom simply because the octahedra in KNNs are fairly rigid. The sense, i.e., direction, of Nb off-centering would change accordingly, and KNNs in the Na-rich side of the phase diagram would behave as ferroelectrics [7,8,11,12]. Cavities around a "guest" K atom would also change in size to a certain extent so that the local tensile strain generated by the replacement is relieved as much as possible. In turn, tilts of octahedra surrounding those cavities would also change to a certain extent, leading to local variations in the octahedral tilts pattern. Indeed, rotations of joined octahedra and the size of nearby cavities in perovskite lattices are intimately coupled, and changes in one of these quantities would be accompanied by changes in the other. The resulting local structural disorder would reach its maximum value when the ratio of "host" Na and "guest" K atoms in KNNs, i.e., "loose" and "tight" cavities, approaches 1, softening the crystalline lattice and easing the polarization rotation. Further replacement of Na for K would "stiffen" the lattice, and the piezoelectric response would approach that of $KNbO_3$. The same scenario applies when K is the "host" and Na is the "guest" atom in the perovskite lattice. This time, however, Na would be inducing tilts in the initially "tilts-free" perovskite lattice. This scenario does not envisage the presence of a morphotropic boundary, low-symmetry bridging phases, and/or distinct nanoscale domains. It explains the

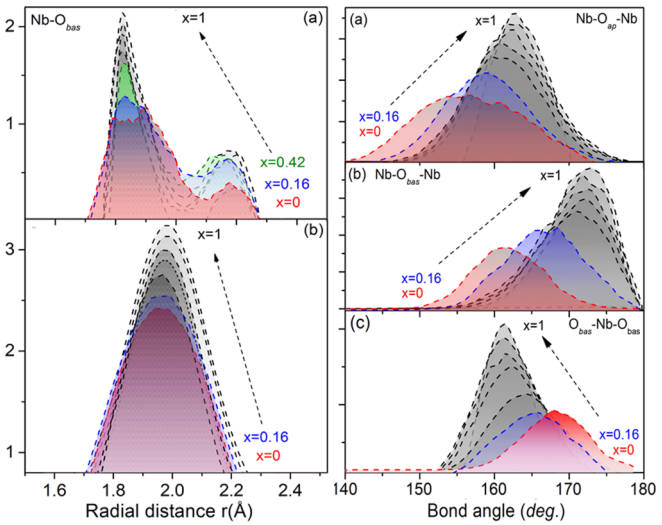

FIG. 7. Left: distribution of (a) Nb-O_{bas} and (b) Nb-O_{ap} distances in Nb-O octahedra in $Na_{1-x}K_xNbO_3$ ferroics ($x = 0$, 0.16, 0.42, 0.52, 0.63, 0.82, and 1). Right: distribution of (a) Nb-O_{ap}-Nb, (b) Nb-O_{bas}-Nb, and (c) O_{bas}-Nb-O_{bas} bond angles in the perovskite lattice of KNNs. Data are extracted from the respective 3D structure models. Note that, as discussed in the text, the rather broad distribution of bonding distances and angles in $NaNbO_3$ arises from the particular Nb off-centering and the presence of pronounced octahedral tilts illustrated in Figs. 5 and 6. Indeed, the latter is what suppresses ferroelectricity in this material.

increased piezoelectric response of KNNs in terms of emerging local fluctuations in octahedral tilts driven by fluctuations in atomic-level stresses. The stresses accumulate locally and reduce the length of structural coherence in $Na_{1-x}K_xNbO_3$ with x $\sim$ 0.5 to distances on the scale of 8–10 nm but appear averaged out at longer distances, leading to a uniform expansion of the perovskite lattice with K percentage [see Fig. 1(c)]. Needless to say, for the mechanisms discussed here for increased piezoelectric response to be optimized for practical applications, the distribution of distinct *A*-atoms (Na and K) in the perovskite lattice ought to be kept as uniform as possible.

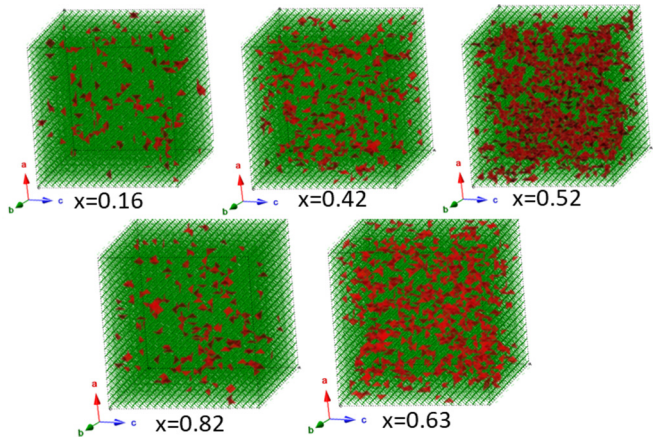

FIG. 8. Octahedral framework (green) of mixed $Na_{1-x}K_xNbO_3$ oxide ferroics ($x = 0.16$, 0.42, 0.52, 0.63, and 0.82). Configurations of Nb-O_6 octahedra tilted differently from the majority of octahedra in the respective model structure are given in brown. Tilts are determined using relevant bond angles and distances between nearby Nb and O atoms as explained in the text.

V. CONCLUDING REMARKS

It has been shown that variations in the geometrical stability of pseudobinary ABO_3 perovskites induced by gradually substituting one *A*-atom for another, such as $Na_xK_{1-x}NbO_3$ ferroics, can be explained in terms of variations in Goldschmidt's tolerance factor related to variations in two important structural parameters. The first is the variation in the average *A*-atom radius, $\langle r_A(x)\rangle = xr_k + (1-x)r_{Na}$, with the K percentage x, where r_{Na} and r_K are the ionic radii of Na and K, respectively. The second is the emergence of local structural disorder due to the size mismatch between the two different types of *A*-ions (Na and K). To a good approximation, the disorder can be described in terms of the statistical variance, σ^2, in the local distribution of $r_A(x)$ radii about $\langle r_A(x)\rangle$, defined as $\sigma^2 = \langle r_A(x)^2\rangle - \langle r_A(x)\rangle^2$ [28–30]. More details are given in the Supplemental Material [18]. As illustrated in Fig. S9 in the Supplemental Material [18], $r_A(x)$ and σ^2 appear as a strictly linear and quadratic function of x, respectively. Thus, it may be expected that the properties of KNNs largely sensitive to changes in the former would evolve linearly with the K percentage, whereas those largely sensitive to the latter would appear as a quadratic function of that percentage. Properties depending on both $r_A(x)$ and σ^2 may appear as an asymmetric, second-degree polynomial function of K percentage of the type shown in Fig. S9(a) in the Supplemental Material [18]. As data in Fig. 9 (right) indicate, the gradual increase in $\langle r_A(x)\rangle$ with K percentage results in a gradual diminishing of the tilts of Nb-O octahedra, as represented by the near-linear evolution of the respective average Nb-oxygen bonding distances and angles, thus stabilizing the ferroelectricity in KNNs. On the other hand, local structural instabilities, such as local fluctuations in the size of the cavities and octahedral tilts, as represented by the nonlinear evolution of the unit cell volume and the respective length of structural coherence, enable the rotation of polarization to occur more easily, thereby increasing the piezoelectric response (constant) of KNNs. Among many others, the well-known $(Ba, Ca)TiO_3$, $Bi(Na, K)TiO_3$, and $(Sr, Ba)MnO_3$ ferroics can also be considered to exhibit enhanced piezoelectric response thanks to local structural instabilities of the type described here [32]. Recent theoretical studies have also pointed out the important role of *A*-atom size, displacement, and related octahedral tilts in both (de)stabilizing the ferroelectricity and enhancing the piezoelectric response in perovskites [14,33]. Thus, local structural disorder and the resulting geometrical frustration in the underlying perovskite lattice appear as important structural characteristics of oxide ferroics that may be rationally utilized in the ongoing effort to improve their functionality.

From a more general point of view, the effect of local disorder in ferroelectrics on their piezoelectric properties may be considered in terms of free-energy instabilities [34–36]. In particular, it is well known that the larger the difference between the size, i.e., volume, of solute and solvent atoms in pseudobinary solid solutions, the greater the tendency away

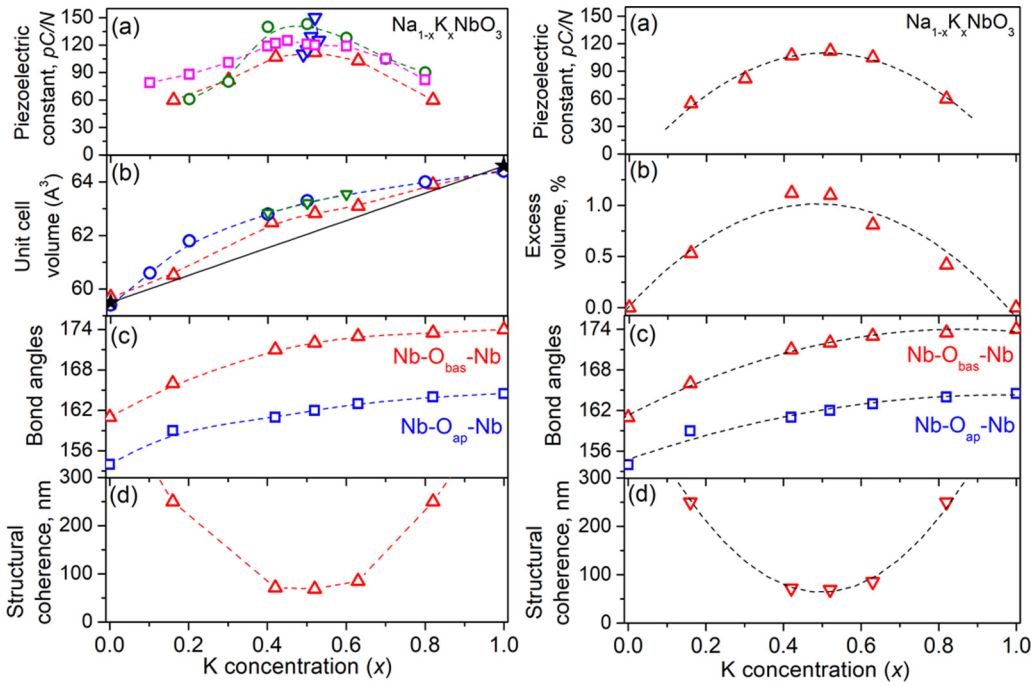

FIG. 9. Left: (a) Experimental data for the piezoelectric constant, d_{33}, of $Na_{1-x}K_xNbO_3$ ferroics ($x = 0.16, 0.42, 0.52, 0.63$, and 0.82). Data from literature sources [39–41] are given as green circles, blue triangles, and magenta squares. Our experimental data are given as red triangles. (b) Experimental data for the volume of the unit cell of $Na_{1-x}K_xNbO_3$ ferroics. Data from literature sources [42,43] are given as blue circles and green triangles. Our data, extracted from fits to experimental PDFs, are given as red triangles. The solid black line connects literature data for the unit cell volume of $NaNbO_3$ and $KNbO_3$. (c) Average bond angles in $Na_{1-x}K_xNbO_3$ ferroics extracted from their 3D structure models. (d) Length of structural coherence in $Na_{1-x}K_xNbO_3$ ferroics obtained from the experimental PDFs in Fig. 1(c). Broken lines in (a), (b), (c), and (d) are a guide to the eye. Right: Our experimental data from the respective plots on the left (symbols) as fit with a second-degree polynomial function of the type $\langle r_A(x)\rangle + x(x+1)(r_K - r_{Na})^2$ (broken black line) [29–31]. Correlation coefficients for the fits to the data are on the order of 0.94(2).

from ideal solution behavior, giving rise, to excess volume of mixing. PDF data for the composition dependence of the volume of the unit cell of KNNs obtained here confirm this assumption. Generally, an increase in volume causes an increase in entropy, thereby a random-type octahedral tilt pattern would appear energetically favorable for KNNs due to its propensity to fluctuate and thus accommodate fluctuations in local stresses arising from the different size of Na and K atoms. Thus, the usual coupling between the polarization direction and high-symmetry axes of the underlying perovskite lattice would be reduced and the piezoelectric response increased. This implies that the search for ferroelectrics with increased functionality need not necessarily concentrate on systems exhibiting transitions between phases with different crystallographic symmetry, low-symmetry bridging phases, and/or distinct polar nanodomains [37]. Inducing local structural disorder in a controlled manner, including engineering local fluctuations in atomic-level stresses through measured cation substitution, may become worthwhile. Engineering of domains with a special configuration, i.e., extrinsic contributions, may increase the pursued functionality further [3–5,38].

ACKNOWLEDGMENTS

This work was supported by the U.S. Department of Energy, Office of Science, Office of Basic Energy Sciences under Award No. DE-SC0006877 and used resources of the Advanced Photon Source at the Argonne National Laboratory provided by the DOE Office of Science under Contract No. DE-AC02-06CH11357. Thanks are due to Y. Maswadeh and L. Hui for the help with the synchrotron XRD experiments.

[1] C. R. Bowen, H. A. Kim, P. M. Weaver, and S. Dunn, Piezoelectric and ferroelectric materials and structures for energy harvesting applications, Energy Environ. Sci. **7**, 25 (2014).

[2] M. T. Chorsi, E. J. Curry, H. T. Chorsi, R. Das, J. Baroody, P. K. Purohit, H. Ilies, and T. D. Nguyen, Piezoelectric biomaterials for sensors and actuators Adv. Mater. **31**, 1802084 (2019).

[3] W. Huige, H. Wang, Y. Xia, C. Dapeng, Y. Shi, Y. Dong, Ch. Kiu, T. Ding, J. Zhang, Y. Ma, N. Wang, A. Wang, Y. Sun, R. Wei, and Z. Guo, An overview of lead-free piezoelectric materials and devices, J. Mater. Chem. C **6**, 12446 (2018).

[4] J.-F. Li, K. Wang, F-Y. Zhu, L-Q. Cheng, and F.-Z Yao, $(K, Na)NbO_3$ lead-free piezoceramics: Fundamental aspects,

processing technologies, and remaining challenges, J. Am. Ceram. Soc. **96**, 3677 (2013).

[5] Q. Liu, Y. Zhang, J. Gao, Z. Zhou, H. Wang, K. Wang, X. Zhang, L. Li, and J.-F. Li, High-performance lead-free piezoelectrics with local structural heterogeneity, Energy Environ. Sci. **11**, 3531 (2018).

[6] A. W. Hewat, Cubic-tetragonal-orthorhombic-rhombohedral ferroelectric transitions in perovskite potassium niobate: Neutron powder profile refinement of the structure J. Phys. C **6**, 2559 (1973).

[7] L. Katz and H. D. Megaw, The structure of potassium niobate at room temperature: The solution of a pseudosymmetric structure by Fourier methods, Acta Crystallogr. **22**, 639 (1967).

[8] A. C. Sakowki-Cowley, K. Lakaszewicz, and H. D. Megaw, The structure of sodium niobate at room temperature, and the problem of reliability in pseudosymmetric structures, Acta Crystallogr. B **25**, 851 (1969).

[9] C. J. Cheon, H. W. Joo, K.-W. Chae, J. S. Kim, S. H. Lee, and T. Kamiyama, Monoclinic ferroelectric NaNbO at room temperature: Crystal structure solved using super high resolution neutron powder diffraction, Mater. Lett. **156**, 214 (2015).

[10] E. Johnston, C. T. Chiu, J. E. Parker, K. S. Knight, P. Lighfoot, and S. E. Ashbrook, The polar phase of $NaNbO_3$: A combined study by powder diffraction, solid-state NMR, and first-principles calculations, J. Am. Chem. Soc. **132**, 8732 (2010).

[11] A. M. Glazer, The classification of tilted octahedra in perovskites, Acta Crystallogr. B **28**, 3384 (1972).

[12] P. M. Woodward, Octahedral tilts in perovskites. Geometrical considerations, Acta Crystallogr. B **53**, 32 (1997).

[13] V. M. Goldschmidt, Die gesetze der krystallochemie, Die Naturwissen. **14**, 477 (1926).

[14] N. A. Benedek and C. Fennie, Why are there so few perovskite ferroelectrics?, J. Phys. Chem. C **117**, 13339 (2013).

[15] M. Ahtee and A. M. Glazer, Lattice parameters and tilted octahedra in sodium-potassium niobate solid solutions, Acta Crystallogr. **A32**, 434 (1976).

[16] D. W. Baker, P. A. Thomas, N. Zhang, and A. M. Glazer, A comprehensive study of the phase diagram of $K_xNa_{1-x}ANbO_3$, Appl. Phys. Lett. **95**, 091903 (2009).

[17] S. Gupta, V. Petkov, and S. Priya, Local atomic structure of $K_xNa_{1-x}NbO_3$ by total XRD, Appl. Phys. Lett. **105**, 232902 (2014).

[18] See Supplemental Material at http://link.aps.org/supplemental/10.1103/PhysRevMaterials.4.014405 for synthesis, experimental and modeling details, and plots with experimental XRD patterns and total and Nb-differential atomic PDFs.

[19] E. Takeshi and S. Billinge, *Under the Brag Peaks: Structural Analysis of Complex Materials* (Pergamon, Oxford, 2012).

[20] V. Petkov, *Pair Distribution Function Analysis in Characterization of Materials* (Wiley, Hoboken, New Jersey, 2012).

[21] V. Petkov, I-K. Jeong, J. S. Chung, M. F. Thorpe, S. Kycia, and S. J. L Billinge, High-Real Space Resolution Measurement of the Local Structure of $In_xGa_{1-x}As$ Semiconductor Alloys Using X-Ray Diffraction, Phys. Rev. Lett. **83**, 4089 (1999).

[22] N. Zhang, H. Yokota, A. M. Glazer, Z. Ren, D. A. Keen, D. S. Keeble, P. A. Thomas, and Z.-G. Ye, The missing boundary in the phase diagram of $PbZr_{1-x}Ti_xO_3$, Nat. Commun. **5**, 5231 (2014).

[23] M. G. Tucker, M. T. Dove, and D. A. Keen, Application of the reverse Monte Carlo method to crystalline materials, J. Appl. Crystallogr. **34**, 630 (2001).

[24] C. A. Yong and A. L. Goodwin, Applications of pair distribution function methods to contemporary problems in materials chemistry, J. Mater. Chem. **21**, 6464 (2011).

[25] V. Petkov, S. M. Selbach, M.-A. Einarsrud, T. Grande, and S. D. Shastri, Melting of Bi-Sublattice in Nanosized $BiFeO_3$ Perovskite by Resonant X-Ray Diffraction, Phys. Rev. Lett. **105**, 185501 (2010).

[26] V. Petkov, S. D. Shastri, J.-W. Kim, S. Shan, J. Luo, J. Wu, and Ch. J. Zhong, Application of differential resonant high-energy X-ray diffraction to three-dimensional structure studies of nanosized materials: A case study of Pt-Pd nanoalloy catalysts, Acta Crystallogr. A **74**, 553 (2018).

[27] I. Levin, V. Krayzman, G. Gibin, M. G. Tucker, M. Eremenko, K. Chapman, and R. K. Paul, Coupling of emergent octahedral rotations to polarization in $(K, Na)NbO_3$ ferroelectrics, Sci. Rep. **7**, 15620 (2017).

[28] A. M. Glazer, P. A. Thomas, K. Z. Baba-Kishi, G. K. H. Pang, and C. W. Tai, Influence of short-range order and long-range order on the evolution of the morphotropic boundary in $Pb(Zr_{1-x}Ti_x)O_3$, Phys. Rev. B **70**, 184123 (2004).

[29] J. P. Attfield, A simple approach to lattice effects in conducting perovskite oxides, Chem. Mater. **10**, 3239 (1998).

[30] J. P. Attfield, L. Kharlanov, and J. A. McAllister, Cation effects in doped La_2CuO_4 superconductors, Nature (London) **394**, 157 (1998).

[31] D. C. Sinclair and J. P. Attfield, The influence of A-cation disorder on the Curie temperature of ferroelectric $ATiO_3$ perovskites, Chem. Commun. **16**, 1497 (1999).

[32] X. Hao, A Review on the dielectric materials for high energy-storage applications, J. Adv. Dielectrics **03**, 1330001 (2013).

[33] T. A. Mulder, N. A. Benedek, J. M. Rondinelli, and C. J. Fennie, Turning ABO antiferroelectrics into ferroelectrics: Design rules for practical rotation-driven ferroelectricity in double perovskites and $A_3B_2O_7$ Ruddlesden-Popper compounds, Adv. Funct. Matter. **23**, 4810 (2013).

[34] A. G. Khhachaturya, Ferroelectric solid solutions with morphotropic boundary: Rotational instability of polarization, metastable coexistence of phases and nanodomain adaptive states, Philos. Mag. **90**, 37 (2010).

[35] D. Damjanovic, Comments on origins of enhanced piezoelectric properties in ferroelectrics, IEEE Trans. Ultrason., Ferroelectr., Freq. Control. **56**, 1574 (2009).

[36] V. K. Wadhavan, in *Ferroelasticity and Related Properties of Crystals* (Gordon and Breach, Amsterdam, 1983).

[37] J. Wu, D. Xiao, and J. Zhu, Potassium-sodium niobate lead-free piezoelectric materials: Past, present, and future of phase boundaries, Chem. Rev. **115**, 2559 (2015).

[38] S. Gupta, S. Huband, D. S. Keeble, W. Walker, P. Thomas, D. Viehland, and S. Priya, Optical crystallographic study of piezoelectric $K_xNa_{1-x}NbO_3$ ($x = 0.4$, 0.5 and 0.6) single crystals using linear birefringence, CrystEngCommun. **15**, 6790 (2013).

[39] B.-P. Zhang, J.-F. Li, K. Wang, and H. Zhang, Compositional dependence of piezoelectric properties in $Na_xK_{1-x}NbO_3$ lead-free ceramics by spark plasma sintering, J. Am. Ceram. Soc. **89**, 1605 (2006).

[40] Y.-J. Dai, X.-W. Zhang, and K.-P. Chen, Morphotropic boundary and electrical properties of $K_{1-x}Na_xNbO_3$ lead-free ceramics, Appl. Phys. Lett. **94**, 042905 (2009).

[41] L. Wu, J. L. Zhang, C. L. Wang, and J. C. Li, Influence of compositional ratio K/Na on physical properties in $K_{1-x}Na_xNbO_3$ ceramics, J. Appl. Phys. **103**, 084117 (2008).

[42] G. Shirane, R. Newnham, and R Pepinsky, Dielectric properties and phase transitions of $NaNbO_3$ and (Na, K)NbO_3, Phys. Rev. B. **96**, 581 (1954).

[43] B. M. Tellier, B. Dkhil, D. Jenko, J. Cilensek, and M. Kosec, Crystal structure and phase transitions of sodium potassium niobate perovskites, Solid State Sci. **11**, 320 (2009).